



Identification of Structure Activity Relation of A Synthetic Drug 2,6-Pyridine Dicarbonitrile Using Experimental And Theoretical Investigation

G.Golding Sheeba^{1*}, Shijula lindry¹ R.Mini ², Devi³

¹Department of Science and Humanities, Annai Vailankanni College of Engineering, Kanyakumari-629401

²Department of Science and Humanities, Annai Vailankanni College of Engineering, Kanyakumari-629401

³Department of Science and Humanities, Annai Vailankanni College of Engineering, Kanyakumari-629401

⁴Department of Science and Humanities, Annai Vailankanni College of Engineering, Kanyakumari-629401

Abstract

The structural activity relationship of the compound 2,6-pyridinedicarbonitrile has been analyzed by using structural and bonding investigation. The optimized molecular structure of (26PDC) molecule was computed by gradient corrected density functional theory (DFT) method with three parameter hybrid functional Backe 3(B3) for the exchange part and Lee–Yang–Parr (LYP) correlation function level of theory using Gaussian 09 program package with 6-311++G (d,p) basis sets. The harmonic vibrational wavenumbers for 2,6PDC have been calculated by using the DFT method at 6-311++G (d,p) level. The calculated HOMO - LUMO band gap energies confirm that charge transfer occurs within the molecule.

Keywords: DFT, Molecular structure, NBO, HOMO and LUMO

Introduction:

Pyridine is a basic heterocyclic organic compound with the chemical formula C₅H₅N. It is structurally related to benzene, with one methine group (=CH-) replaced by a nitrogen atom. Most of the Pyridine derivatives are biologically and pharmacologically important molecules. So, the Pyridine derivatives are widely used in the synthesis of various biologically and pharmacologically active molecules. These not only become the subject of great interest due to their diverse biological and medical activities but also because of their other activities. Some of the pyridine derivatives represent an important group of organic compounds that are used as reagents in analytical chemistry. Some of the other pyridine derivatives view anesthetic properties and are used as medicine for some brain diseases. Additionally, they are known to exhibit biologically active antibacterial, antiviral, antifungal, and antitumor properties. These are widely used as agricultural chemical agents such as herbicides, insecticides and fungicides. They are also widely used as agricultural chemical agents such as herbicides, insecticides and fungicides. In medical applications, these compounds share an important part. Pyridine derivatives target different biological problems by interacting with enzymes, proteins and DNA.

In recent years density functional theory (DFT) has become a powerful tool in the investigation of molecular geometrical structures. The vibrational spectra with density functional theory (DFT) calculation have been used as an effective tool in the functional group analysis of drugs, biological and NLO active materials. The DFT calculations are powerful and very reliable tools for calculating various molecular properties. DFT is a **universally** useful computational



method and can be connected to various systems. Moreover, DFT methods are more helpful for certain kinds of computations than others. Furthermore, DFT can be utilized for computations including metals. Several DFT methods, for example, B3LYP, are specially planned for specific applications. The structural, thermal and spectroscopic investigations of pyridine and its derivatives attract many researchers due to its wide range of applications. In the present work, the molecular structure of 2, 6-pyridine dicarbonitrile (26PDC) was optimized by the DFT/B3LYP method. The characteristic vibrational wavenumbers of the molecule were experimentally observed and theoretically calculated. The vibrational wavenumbers were assigned based on potential energy distribution (PED) calculation using VEDA 4 program. The Mulliken and natural atomic charge distribution were also calculated. The Frontier molecular orbitals (FMOs) analysis was reported to study the molecular reactivity and stability of the molecule. The natural bond orbital (NBO) analysis was also carried out to understand the bonding features of the molecule.

5.2 Experimental details:

The FT-IR spectrum of (26PDC) molecule was recorded in the region 4000–400 cm^{-1} on Perkin Elmer spectrophotometer using KBr pellet. The spectral resolution is $\pm 1 \text{ cm}^{-1}$. The FT-Raman spectrum of (26PDC) molecule has been recorded with Bruker BRUKER: RFS 27 in the region 50–3500 cm^{-1} using 1064 nm line of Nd:YAG laser as excitation. The spectra were recorded with a spectral resolution of 2 cm^{-1} .

5.3 Computational details

The optimized molecular structure of (26PDC) molecule was computed by gradient corrected density functional theory (DFT) method with three parameter hybrid functional Becke 3(B3) for the exchange part and Lee–Yang–Parr (LYP) correlation function level of theory using Gaussian 09 program package with 6-311++G (d,p) basis sets. The molecular structure, vibrational spectra, Mulliken atomic charge distribution, surface contour map and FMOs were visualized by GaussView 05 visualizing program. The most stable optimized structure of the molecule was predicted by the DFT/B3LYP method with 6-311++G (d,p) basis set. The vibrational frequencies, Mulliken atomic charge distribution, FMOs, thermodynamic parameters, first order hyperpolarizability and NBO calculations were carried out for the optimized structure of the molecule by the DFT/B3LYP method with 6-311++G (d,p) basis set. These calculations were done at the ground state energy level of the (26PDC) molecule without applying any constraint on the potential energy surface. The vibrational modes were assigned with a high degree of accuracy based on potential energy distribution (PED) calculation using the VEDA4.0 program and visualized by Gauss View 05 program. The electron localization function (ELF), Localized orbital locator (LOL) AIM, analysis, Reduced Density Gradient (RDG) and bond order analysis of the title molecule are done by Multiwfn [29] and plotted by the VMD program [30].

Optimized geometry:

The optimized geometric structure of the molecule 26PDC has been performed using B3LYP method and indicated in Figure 5.1. The Theoretically geometric parameters (dihedral angles, bond lengths and bond angles) have been calculated and given in Table 5.1. It shows that all the geometries determined belong to a true minimum proven by real wavenumbers in the vibrational analysis. From the table, it shows that all the bond length, bond angle and dihedral are within the limits. 2,6- Pyridine dicarbonitrile compound consists of 5C-C bond, 4C-N bond and 3C-H bond. In that the C-C bond length ranges from 1.3922Å to 1.439Å. The C-N bond length ranges from 1.153Å to 1.336Å.

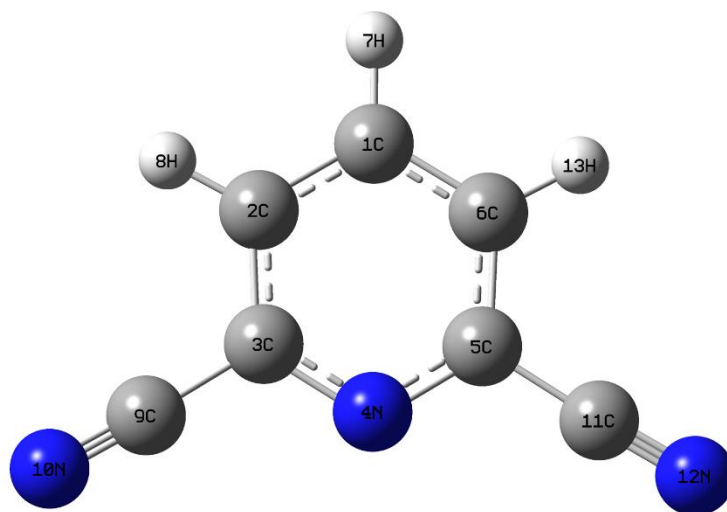


Figure 5.1. Optimized structure of 26PDC calculated at DFT level

Tables 5.1: Optimized geometrical parameters of (26PDC) calculation of B3LYP/6-31 G(d,p) level

Bond Length	Value (Å)	Bond Angle	Value (°)	Dihedral Angle	Value (°)
C ₁ -C ₂	1.392	C1-C2-C3	118.1	C1-C2-C3-N4	0.0
C ₂ -C ₃	1.403	C2-C3-N4	123.9	C2-C3-N4-C5	0.0
C ₃ -N ₄	1.339	C3-N4-C5	116.8	C3-N4-C5-C6	0.0
N ₄ -C ₅	1.339	N4-C5-C6	123.9	C3-C2-C1-H7	180.0
C ₅ -C ₆	1.403	C2-C1-H7	120.5	N4-C3-C2-H8	180.0
C ₁ -H ₇	1.085	C3-C2-H8	120.1	C1-C2-C3-C9	180.0



C ₂ -H ₈	1.084	C2-C3-C9	119.4	C2-C3-C9-N10	180.0
C ₃ -C ₉	1.443	C3-C9-N10	177.8	C3-N4-C5-C11	180.0
C ₉ -N ₁₀	1.161	N4-C5-C11	116.6	N4-C5-C11-N12	180.0
C ₅ -C ₁₁	1.443	C5-C11-N12	177.8	N4-C5-C6-H13	180.0
C ₁₁ -N ₁₂	1.161	C5-C6-H13	120.1		
C ₆ -H ₁₃	1.084				

The C-H bond length ranges from 1.082 Å to 1.023 Å. In the pyridine ring, the bond length C₂-C₃ (1.400Å) and C₅-C₆ (1.400Å) are more extended than the other C-C value which is due to the combination of pyridine ring and it shows the presence of nitrogen atom within the ring. Thus, the bond length C₃-C₉ (1.441Å) and C₅-C₁₁ (1.441Å) are also extended more than all other C-C value. It shows the possibility of electron transfer from the ring to carbonitrile nitrogen. From all the C-N bond lengths, the C₉-N₁₀ (1.161Å) and C₁₁-N₁₂ (1.133Å) are more contracted than the other C-N bond lengths. This contraction is due to the triple bond nature of C-N bond length. Both C3-N4 and N4-C5 have 1.356 Å, it is longer than the other bond length and shows the possibility of single bond character. All the C-H atoms are well within the limit. The endocyclic angle C₂-C₃-N₄ is larger than the normal value and exocyclic angle is lesser than the normal value. The bond angles C₃-N₄-C₅ and N₄-C₅-C₁₁ are also decreased than the normal value. All the dihedral angles ranges from 0.0° to 180.0°. It shows the planar surface of the molecule. There is no twisting that takes place between the ring and the other compounds.

Vibrational Analysis:

The harmonic vibrational wavenumbers for 2,6PDC have been calculated by using the DFT method at 6-311++G (d,p) level. As a result of theoretical calculations, there are no imaginary values for any frequencies. All of the calculated frequencies with DFT are scaled by 0.96 to compare with experimental frequencies. The bands in the experimental and stimulated FT-IR and FT-Raman spectra of the title compound are illustrated in [Figure 5.2 and 5.3](#) respectively, and some characteristic frequencies are tabulated in [Table 5.3](#). As seen in [Table 5.3](#), the calculated frequencies are slight differed from the experimental values. The reason for these small differences may be the neglect of anharmonicity in DFT calculations. Furthermore, the vibrational frequencies are affected by the environment in which the molecule is located. These differences are not surprising since the calculated vibrational modes are calculated for a single molecule in the gas phase.

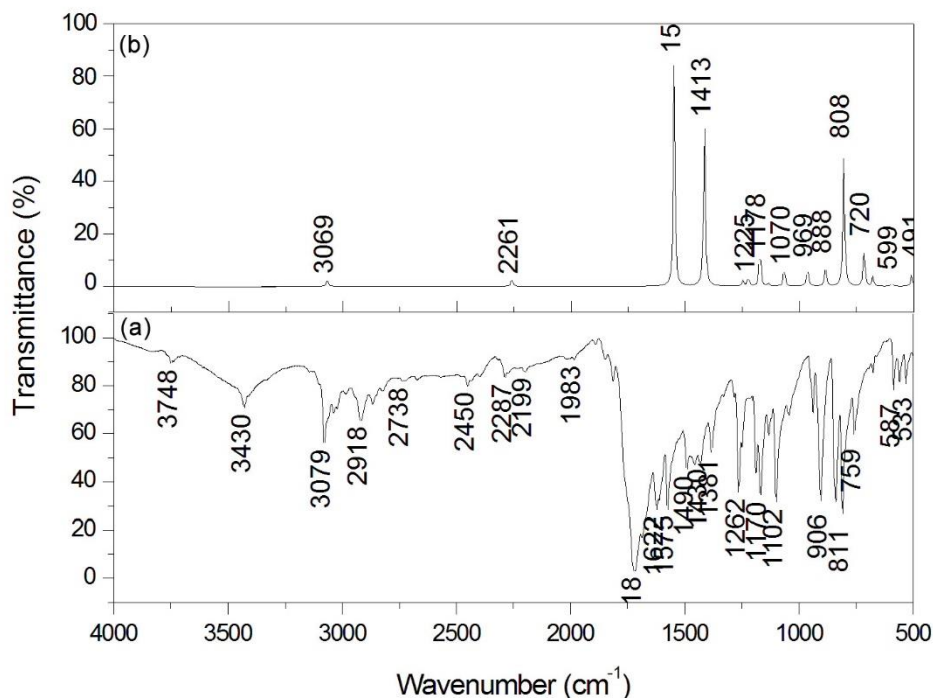


Figure: (a) Experimental and (b) Stimulated FT-IR spectrum of 26PDC in the region 50-4000 cm^{-1}

C-C Vibration:

The C-C stretching vibrations in the benzene derivatives appear in the range of 1650-1590 cm^{-1} [35,36]. In our compound, the C-C stretching vibration is observed in IR at 1575 cm^{-1} and in Raman at 1555 cm^{-1} . The assigned value is shifted away from the range. The shift of wavenumber with the mass of substitution has been reverse in these modes. This shows that, there is a gain in energy instead of a loss as it is in the previous cases [37,38]. In the present case, ring C-C stretching vibrations are suppressed due to the bonding of N in the ring. Several C-C in plane and out-of-plane bending vibration modes of the ring carbons are expected. Due to the high symmetry of the benzene ring, any modes of vibrations are infrared inactive[39]. In general, the bands of variable intensity are observed at 841,811,674 cm^{-1} in IR and 863,821,635 cm^{-1} in Raman.

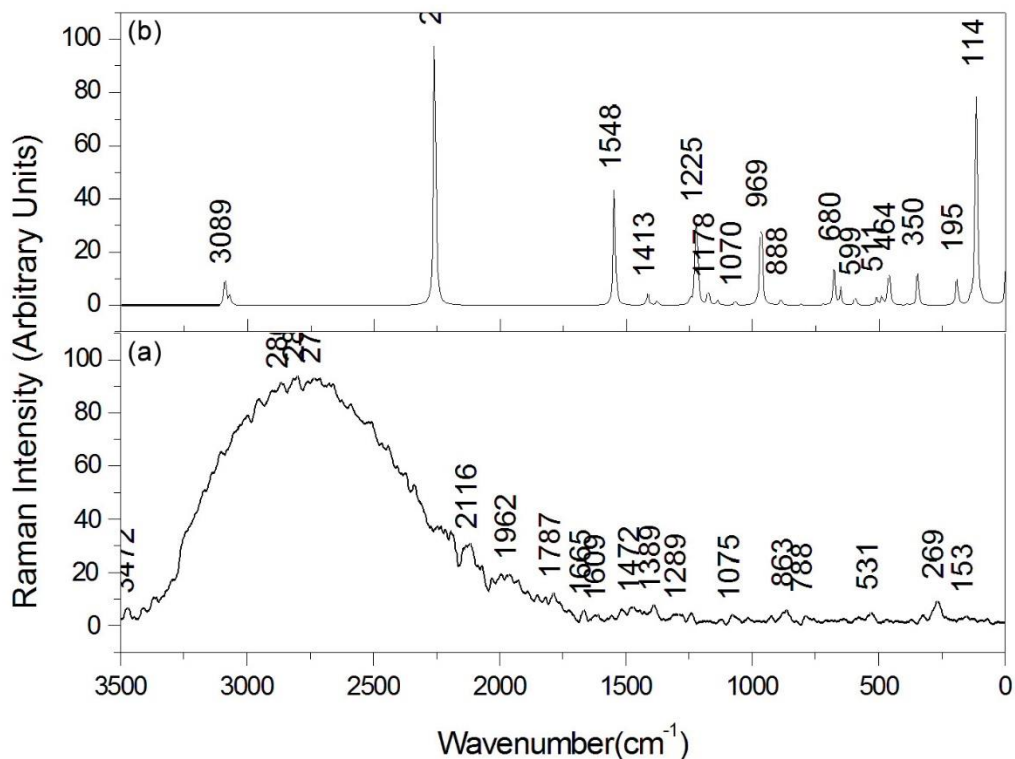


Figure (a) Experimental and (b) Stimulated FT-Raman spectrum of 26PDC in the region 50-4000cm⁻¹

C-H Vibration:

The hetero aromatic organic compounds commonly exhibit multiple weak bands in the region 3100–3000cm⁻¹ due to C–H stretching vibrations. In our compound, the C-H stretching vibration is observed in IR at 3079 and 3043 cm⁻¹ and in Raman at 3051cm⁻¹. The C-H in plane bending vibrations have been appeared in the range of 1000-1300cm⁻¹ and are very useful for characterization purposes.

Comparison of the experimental (FT-IR, FT-Raman) wavenumbers (cm⁻¹) and theoretical wavenumbers (cm⁻¹) of 2PDC calculated by B3LYP/6-311++G(d,p) level of theory.

Cal.	FTIR	FT Raman	Assignments
3087	3079 m		C1-H7 Stretching (96)
3082			C2-H8 Stretching (99)



3067	3043 vw	3051 m	C1-H7 Stretching (97)
2259		2231 m	N10-C9 Stretching (90) +C3-C9 Stretching (13)
2258	2287 w	2250 m	N10-C9 Stretching (89)
1547	1575 s	1555 w	C2-C3 Stretching (52) +H13-C6-C1 Bending(16) +C2-C1-C6 Bending (12) +C3-N4-C5 Bending (10)
1547		1517 w	C1-C2 Stretching (74) +H7-C1-C6 Bending (16)
1414	1430 m	1430 w	C2-C3-N4 Bending (12) +H7-C1-C6 Bending (60)
1377	1381 m	1389 w	C1-C2 Stretching (72) +H13-C6-C1 Bending (15)
1246	1282 w	1289 w	C1-C2 Stretching (79)
1222	1262 S	1242 w	N4-C3 Stretching (16) +C3-C9 Stretching (28) + H13-C6-C1 Bending(13) +C2-C1-C6 Bending (14) +C3-N4-C5 Bending (19)
1174	1170 s	1122 vw	C3-C9 Stretching (18) +C2-C3-N4 Bending (14) +H7-C1-C6 Bending (38) +C3-C9-N10 Bending (10)
1138	1134 w		C1-C2 Stretching (17) +C1-C2 Stretching (11) + H7-C1-C6 Bending (66)
1067	1043 w	1075 w	C2-C3 Stretching (29) +H13-C6-C1 Bending (50)
981		930 w	H7-C1-C2-C3 Torsing(11) +H7-C1-C6-C5 Torsing(70)
965			N4-C3 Stretching (60) +C2-C3-N4 Stretching (14)
908	906 s		H8-C2-C3-N4 Torsing(80) +C1-C6-C5-N4 Torsing (12)
885	841 s	863 w	C3-C9 Stretching (35) +C1-C2-C3 Bending (38)



806	811 s	821 vw	H7-C1-C2-C3 Torsing(56) +H7-C1-C6-C5 Torsing(10) +C1-C6-C5-N4 Torsing(11) +C9-C2-N4-C3 OUT (14)
718	759 m	788 vw	H7-C1-C2-C3 Torsing(26) +H7-C1-C6-C5 Torsing(18) +C- C3-N4-C5 Torsing (43)
679	674 vw	635 vw	C2-C1-C6 Bending (59) +C3-N4-C5 Bending (11)
653	694 w		H8-C2-C3-N4 Torsing(12) +C2-C3-C9-N10 Torsing(29) +C1-C6-C5-N4 Torsing(26) + C1-C6-C5-C11 Torsing (31)
595	587 w		C1-C2-C3 Bending (10) +C3-C9-N10 Bending (81)
511	535 w	531 w	C3-C9-N10 Bending (11)+C3-N4-C5 Bending (15)+C3-C9- N10 Bending (67)
488	498 vw		C2-C3-C9-N10 Torsing(51) +C2-C3-N4-C5 Torsing(12) +C9-C2-N4-C3 OUT (22)
463			C3-C9 Stretching (35) +C2-C3-N4 Bending (41)
461	453 vw	471 vw	C3-C9 Stretching (44) +C2-C3-N4 Bending (33)
389	363 w	370 vw	C2-C3-C9-N10 Torsing (19) +C1-C2-C3-N4 Torsing (76)
349		321 vw	C2-C3-C9-N10 Torsing(56) +C2-C3-N4-C5 Torsing(13) +C1-C6-C5-N4 Torsing (21)
192		153 vw	C3-C9-N10 Bending (96)
140			C2-C3-C9-N10 Torsing (14) +C2-C3-N4-C5 Torsing(10) +C1-C6-C5-C11 Torsing (65)
124			C2-C3-C9-N10 Torsing (26) +C1-C2-C3-N4 Torsing(12) +C9-C2-N4-C3 OUT (58)



116			C3-C9-N10 Bending (84) +C3-C9-N10 Bending (12)
-----	--	--	--

The observed series of strong bands in IR at 1262, 1170 and weak bands in IR at 1134, 1043 cm^{-1} are assigned to the C-H in plane bending vibration. The same mode of vibration is observed in Raman at 1242, 1122, 1075 cm^{-1} as a weak band. The C-H out of plane bending vibrations occur in the region 1000-750 cm^{-1} [45]. The aromatic C-H out of plane bending of EBDA are assigned to the bands observed at 906 cm^{-1} , 811 cm^{-1} in the FT-IR spectrum and in FT-Raman spectrum at 821 cm^{-1} . The theoretically computed wavenumbers of C-H vibrations calculated by B3LYP/6-311++G (d, p) methods show excellent agreement with the recorded spectrum as well as literature data

C-N Vibration:

The identification of ring C-N stretching vibration is a very difficult task because the mixing of several vibrational modes is possible in this region. The C-N stretching vibration is always mixed with other bands and is usually assigned in the region 1266–1382 cm^{-1} [47,48]. In the present investigation, the C-N stretching vibration is observed in IR at 1262 cm^{-1} and in Raman at 1242 cm^{-1} and both are observed and mixed with C-H in-plane bending vibration. The C-N stretching vibration is also observed at the lower end of the expected range which may be due to the interaction of C-C vibration, whose frequency extends up to this value [49]. The C-N in-plane bending and C-N out-of-plane bending are observed around 580 and 330 cm^{-1} respectively [36]. The C-N in plane bending is observed in IR at 674 cm^{-1} , 535 cm^{-1} and in Raman at 635 cm^{-1} , 531 cm^{-1} as a weak band. In C-N out of plane bending is observed in IR at 362 cm^{-1} and in Raman at 370 and 321 cm^{-1} .

5.7 Frontier molecular orbitals (FMOs) analysis

The highest occupied molecular orbital (HOMO) and the lowest unoccupied molecular orbital (LUMO) are called FMOs, which are used to determine the way in which a molecule interacts with other species. The HOMO energy characterizes the ability of electron giving and LUMO energy characterizes the ability of electron-accepting. The energy gap between HOMO and LUMO characterizes the molecular chemical stability and electron conductivity, which is the result of a significant degree of ICT from the end-capping electron donor groups to the efficient electron acceptor groups through π -conjugated path [50]. The HOMO and LUMO orbitals of 26PDC molecule were computed by the DFT/B3LYP method with 6311++G(d,p) basis set and visualized in Figure 5.4. The FMOs analysis of 26PDC molecule shows the delocalization of

changes occur within the molecule, which increases the molecular reactivity of the molecule. It also shows that HOMO charges are accumulated in the C-C atom and in LUMO the charges are localized in Nitrogen atom. The HOMO–LUMO energy gap was calculated as 5.590 eV. The lower energy gap indicates that the strong hydrogen bonding between the charged species reduces the energy gap considerably with the formation of the charge transfer axis. This charge transfer interaction is substantiating the anticancer activity of the molecule.

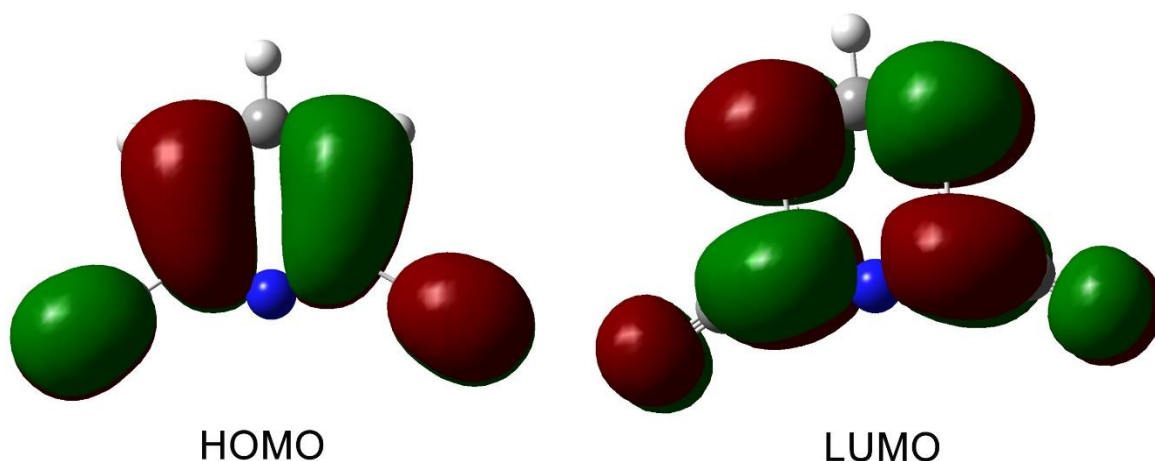


Figure 5.4: FMO plot of 26PDC

Molecular electrostatic potential

Molecular electrostatic potential (MESP) at a point in the space around a molecule gives an indication of the net electrostatic effect produced at that point by the total charge distribution (electron + nuclei) of the molecule and correlates with dipole moments, electronegativity, partial charges and chemical reactivity of the molecule. It provides a visual method to understand the relative polarity of the molecule. It displays the reactivity according to the colors of the region for electrophilic attack and the regions for nucleophilic attack [53].

An electron density isosurface mapped with electrostatic potential surface depicts the size, shape, charge density and site of chemical reactivity of the molecule. Such a mapped electrostatic potential surface has been plotted for the title molecule in 6-311++ G(d,p) basis set using the computer software Gauss view [27]. The MESP plot of 26PDC is shown in the figure 5.5. The different values of the electrostatic potential at the surface are represented by different colors: red represents regions of most negative electrostatic potential, blue represents region of most positive electrostatic potential and green represents region of zero potential. Potential increases in the order: red < orange < yellow < green < blue. In all cases, the shape of the electrostatic potential surface is influenced by the structure and charge density distributions

in the molecule with sites close to the oxygen atom, showing regions to most of the negative electrostatic potential. The calculated 3D MEP shows that the negative regions are electrophilic region; these are mainly due to N atoms. The positive regions are the nucleophilic region and these are over the hydrogen C-H atoms of the title molecule 26PDC. It shows that the potential has been used primarily for predicting sites and relative reactivities towards electrophilic attack and in studies of biological recognition and hydrogen bonding interactions. The potential region varies between $-0.052 e$ to $+0.052 e$

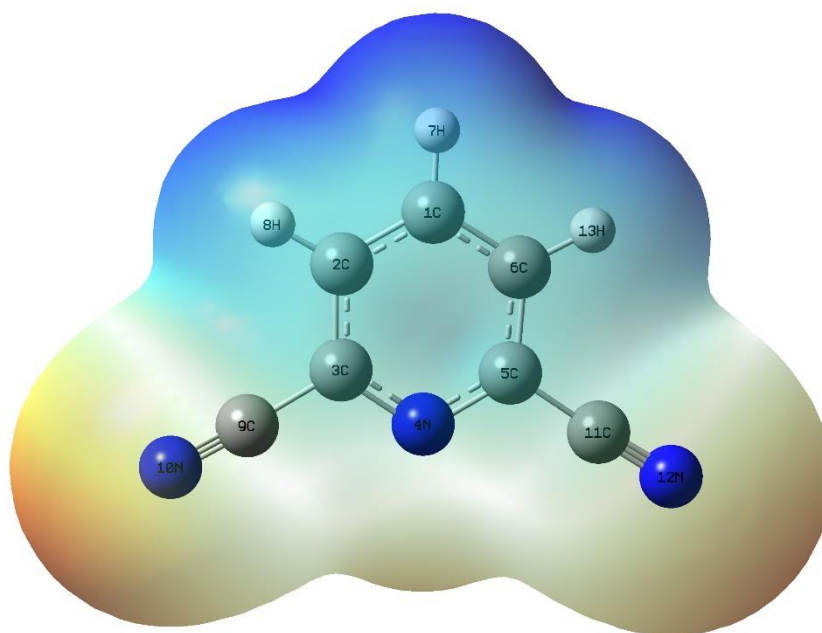


Figure 5.5: MESP plot of 26PDC

Mulliken and Natural population analysis

The natural atomic charge has an important role in the application of quantum mechanical calculation for the molecular system. The natural population analysis of 26PDC is obtained by Mulliken [54] and natural population analysis with B3LYP level using 6-311++G(d,p). method is shown in Figure 5.6 and given in Table 5.4.

Most of the Mulliken show positive charge and some negative charges are observed. In carbon atom, the highest positive charge occurred is C_3 & C_5 ($0.552e$) and the lowest positive charge occurred is C_2 & C_6 ($0.389e$). And in carbon atom, the negative positive charge occurred is C_9 & C_{11} ($-0.818e$) and the lowest negative charge occurred is C_1 ($-0.728e$). In nitrogen atom, the highest and lowest positive charge occurred is N_4 ($0.168e$). And in nitrogen atom the highest and the lowest positive charge occurred are N_{10} & N_{12} ($-0.184e$). In Mulliken, all the hydrogen

atom has only positive charge. In hydrogen atom the highest charge occurred is H₈ & H₁₃ (0.241e) and the lowest charge occurred is H₇ (0.199e).

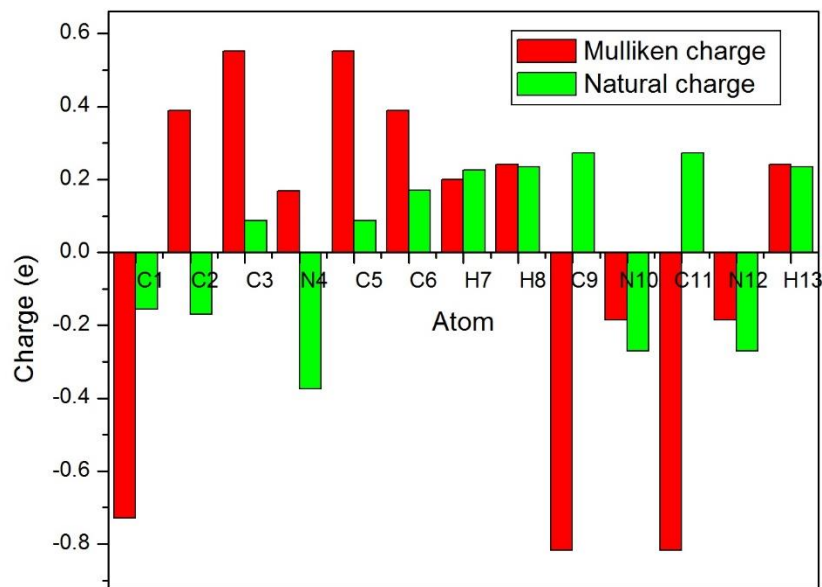


Figure 5.6. Mulliken and natural charges of 26PDC

In natural charge some positive values are observed for some of the atom. The highest positive charge occurs in C₉ & C₄ (0.272e) and the lowest positive charge occurs in C₃ & C₅ (0.087e). The highest positive charge occurred in carbon atom is C₂ & C₆ (-0.170e) and the lowest positive charge occurred in C₁ (-0.155e). Most of the nitrogen atom has a positive charge. The highest negative charge occurs in N₄ (-0.374e) and the lowest negative charge occurs in N₁₀ & N₁₂ (-0.270e). Most of the hydrogen atoms have positive charge. The highest positive charge that occurred in hydrogen atom is H₈ & H₁₃ (0.233e) and the lowest positive charge occurred in hydrogen atom is H₇ (0.225e).

Table 5.4: Mulliken and natural Atomic Charges of 26PDC:

Atom	Mulliken Charge (e)	Natural Charge (e)
C1	-0.728	-0.155
C2	0.389	-0.170
C3	0.552	0.087
N4	0.168	-0.374
C5	0.552	0.087
C6	0.389	0.170
H7	0.199	0.225

H8	0.241	0.233
C9	-0.818	0.272
N10	-0.184	-0.270
C11	-0.818	0.272
N12	-0.184	-0.270
H13	0.241	0.233

Conclusions:

Geometric optimization, FT-IR spectra have been computed by DFT using B3LYP/6-311G++(d,p) level of theory and basis set. The result shows that there is a good agreement between the experimental and theoretical data indicating the validity of the DFT level of theory and basis applied to 2,6pyridinedicarbonitrile molecule for prediction of both structural and spectroscopic data of the title compound. The vibrational assignments of the molecules have been calculated and analyzed. The electron cloud movement of the molecule is identified by molecular electrostatic potential. The HOMO and LUMO energies of 2,6pyridinedicarbonitrile molecules were calculated. The HOMO-LUMO energy gap is low. The lower energy gap indicates the possibility of strong intramolecular charge transfer species that reduces the energy gap considerably with the formation of the charge transfer axis, which is the measure of anti cancer activity of the molecule. The presence of Pauli repulsion was identified using the electron delocalisation analysis.

References:

1. Tranfic, M., Halambek, J., Cetina, M., Jukic M. (2011). Synthesis, X-ray and spectroscopic analysis of 2-hydrazino-6-methyl-4-(methoxymethyl)-5-nitropyridine-3-carbonitrile. *Journal of Molecular Structure*, 1001, 145-151.
2. Ataf Ali Altaf, Adnan Shahzad, Zarif Gul, Nasir Rasool, Amin Badshah, Bhajan Lal, Ezzat Khan (2015). A Review on the Medicinal Importance of Pyridine Derivatives. *Journal of Drug Design and Medicinal Chemistry* 1(1), 1-11
3. Mauro Vieira De Almeida, Marcus Vinicius de Nora Souza, Nadia Rezende Barbosa, Frederico Pittella Silva, Giovanni Wilson Amarante, Sílvia Helena Cardoso. (2007). Synthesis and Antimicrobial Activity of Pyridine Derivatives Substituted at C-2 and C-6 Positions. *Letters in Drug Design & Discovery* ,4 (2) 2 , 149 – 153.
4. Looga A.M., Ambassa P., Kamga .J, Hortense G.K., Ngadjui B.T. and Ngameni B. (2019) Synthesis and Evaluation of Antimicrobial Properties of Some Novel Indole



Pyridine Based Chalcones., Austin Journal of Analytical Pharmaceutical Chemistry; 6(2): 1116-1121.

5. Wayne K. Anderson, Dennis C. Dean, and Toshiyasu Endo. (1990) Vinylogous carbinolamine tumor inhibitors. Synthesis, chemistry, and antineoplastic activity of .alpha.-halopyridinium salts: potential pyridone prodrugs of acylated vinylogous. carbinolamine tumor inhibitors. Journal of Medicinal Chemistry, 33(6), 1667-1675
6. Author links open overlay panelJung-NyoungHeoYoung SeobSongBum TaeKim.2005(). Microwave-promoted synthesis of amino-substituted 2-pyridone derivatives via palladium-catalyzed amination reaction. Tetrahedron Letters Volume 46, 4621-4625
7. Heo J.N., Song Y.S., Kim B.T. (2005). Microwave-promoted synthesis of amino-substituted 2-pyridone derivatives via palladium-catalyzed amination reaction *Tetrahedron Letters*, 46, 4621-4625.
8. Comins D.L.& Nolan J.M. (2001). A practical six-step synthesis of (S)-Camptothecin. *Organic Letters*. 3, 4255-4257.